Numerical Solution of Periodic Transonic Flow through a Fan Stage

J. I. Erdos* and E. Alzner†
General Applied Science Laboratories, Inc., Westbury, N.Y.
and
W. McNally‡
NASA Lewis Research Center, Cleveland, Ohio

A numerical method of solution of the inviscid, compressible, two-dimensional, unsteady flow on a blade-to-blade stream surface through a stage (rotor and stator), or a single blade row, of an axial flow compressor or fan is described. A cyclic procedure has been developed for representation of adjacent blade-to-blade passages, which asymptotically achieves the correct phase between all passages of a stage. A shock-capturing finite-difference method is employed in the interior of the passage, and a method-of-characteristics technique is used at the boundaries. The blade slipstreams form two of the passage boundaries, and are treated as moving contact surfaces capable of supporting jumps in entropy and tangential velocity. The Kutta condition is imposed by requiring the slipstreams to originate at the trailing edges which are assumed to be sharp. Results are presented for a transonic fan stage. The rotor tip section solution is compared with an experimental pressure contour map. The subcritical stator solution is compared with results from a stream function method. Finally, the periodic solution for the stage, which has 44 rotor blades and 46 stator blades, is discussed.

Nomenclature

a = speed of sound $(\gamma p/\rho)^{1/2}$, m/sec
$A,B,C,\ldots,Q$ = position of characteristic and stream path locations (see subscripts)
b = stream surface thickness, m
c = chord length (measured axially), m
c_v = specific heat at constant volume, N·m/kg·K
e = static internal energy per unit mass, N·m/kg
E = absolute total internal energy per unit mass, N·m/kg
E' = relative total internal energy per unit mass, N·m/kg
h = static enthalpy per unit mass, N·m/kg
H = absolute total enthalpy per unit mass, N·m/kg
H' = relative total enthalpy per unit mass, N·m/kg
JS = index of grid column corresponding to $\sigma = 1$
KS = index of grid row corresponding to $\nu = 1$
m = meridional distance, m
n = normal distance, m
N_i = number of blades in ith blade row
p = static pressure, N/m^2
q = magnitude of the velocity vector, m/sec
r = radius, m
R = radius of curvature of slipstream, m
R = gas constant, N·m/kg·K
s = distance along stream path, m
S = entropy per unit mass, N·m/kg·K
t = time, sec
T = static temperature, K
u = meridional velocity component, m/sec
v = relative circumferential velocity component, m/sec
V = absolute velocity vector, m/sec
V_m = meridional velocity component, m/sec
V_θ = absolute circumferential velocity component, m/sec
x = meridional distance, m
y = relative circumferential distance, m
z = axial distance, m
γ = ratio of specific heats
ζ = radial component of vorticity vector, sec^{-1}
η = nondimensional distance normal to a particular surface point
θ = absolute circumferential angle, rad
ν = normalized circumferential coordinate (either absolute or relative)
ξ = nondimensional distance along a tangent to a particular surface point
ρ = static density, kg/m^3
σ = normalized axial coordinate
τ = nondimensional time
ϕ = slipstream or stream path angle, measured on stream surface with respect to meridional coordinate, rad
ω = vorticity vector, sec^{-1}
Ω = angular velocity of rotating blade row, rad/sec

Subscripts

$a,b,c,\ldots,q$ = evaluated at points A,B,C,D,E,F,O,Q, in Figs. 3 and 4
i = index identifying computational domain
j = index identifying grid columns
k = index identifying grid rows
ℓ = lower boundary of blade-to-blade passage (which includes the upper surface of the lower blade of a blade-to-blade passage)
o = reference state, or evaluated at a grid point under consideration
R = rotor
S = stator
u = upper boundary of blade-to-blade passage (which includes the lower surface of the upper blade of a blade-to-blade passage)
1 = first blade row

Presented as Paper 76-369 at the AIAA 9th Fluid and Plasma Dynamics Conference, San Diego, Calif., July 14-16, 1976; submitted Aug. 4, 1976; revision received July 26, 1977.
Index categories: Nonsteady Aerodynamics; Transonic Flow; Computational Methods.
*Vice President and Senior Research Scientist. Member AIAA.
†Research Scientist. Now with Philips Medical Systems, Inc., Shelton, Conn.
‡Research Engineer.

2 = second blade row

Superscript

– = surface-oriented coordinate system (e.g., $\bar{u}$, $\bar{v}$ are velocity components tangent and normal to the blade or slipstream surface, and $\bar{x}$, $\bar{y}$ are the corresponding coordinates)

Introduction

THE flowfield within advanced axial flow turbomachinery is characterized by the presence of mixed subsonic, transonic, and/or supersonic regions; multiple shock waves; shock/boundary-layer interactions; and significant effects of three dimensionality and unsteadiness of the flow. Although significant progress in numerical analysis of internal flows has been made in the last few years, a considerable amount of work remains to attain full predictive capability in this problem area.

The present study has been directed toward development of a numerical method of solution of the complete unsteady equations of motion for a compressible, two-dimensional flow through a compressor or fan. The objective is attainment of a steady solution for a single blade row, or a periodic solution for an interacting pair of blade rows in a stage. Either case may include mixed subsonic, transonic, and/or supersonic flow containing embedded shock waves.

The analysis is formulated with respect to a blade-to-blade stream surface, as depicted in Fig. 1. The inlet and discharge boundary conditions are applied at axial stations one or more chord length upstream and downstream of the blade rows. The selected boundary conditions assume subsonic axial velocity at both stations, but admit either choked or unchoked operation of the blade row or stage. For a single blade row, due to circumferential periodicity, the computational domain encompasses that fraction of the flow annulus containing a single blade-to-blade passage. The locations of the boundaries of the blade-to-blade passages may be defined arbitrarily so long as their spacing corresponds to the blade pitch. Downstream of the blade row the blade slipstreams have been selected as appropriate boundaries of the blade-to-blade passages, since components of the solution may be discontinuous across the slipstreams. Upstream of the blade row the boundaries have been conveniently defined as projections of the mean camber lines.

In the case of a stage consisting of a rotating blade row and a stationary blade row, a set of blade-to-blade passages may be defined for the two blade rows. However, the solution will not possess blade-to-blade passage periodicity in both blade rows, except in the limiting case of an equal number of blades in each row which is avoided in practice. It has been established from considerations of the acoustic problem,[1] that the flow pattern in a typical stage ($N_S > N_R$) will rotate in the opposite direction of the rotor at an angular velocity of $N_R\Omega(N_S - N_R)$ and have a circumferential period of $2\pi/(N_S - N_R)$. The solution at any particular passage at one instant can, therefore, be related to that in another passage at an earlier time. This phase lag forms the basis of a cyclic procedure developed herein for relating the conditions along the boundaries of the computational domain to the solution within the domain at an earlier time.

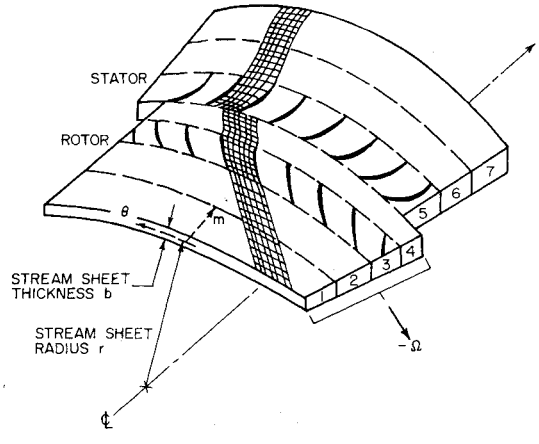

Fig. 1 Blade-to-blade coordinate system and grid network.

The total pressure losses due to boundary layers on the blades will be carried in the wakes of the blades. Thus, a significant contribution to the unsteady aerodynamic interaction between blade rows and resulting acoustic signals may be attributable to passage of one row through the viscous wakes of the other row. Accordingly, approximate representations of the boundary layers on the blade surfaces and the blade wakes have been incorporated in the computational model,[2] but will not be included in the present discussion or results, which, for brevity, are restricted to inviscid flow.

Analysis

Fundamental System of Equations

The basic system from which the equations of this analysis are derived consists of the familiar statements of conservation of mass, momentum, and energy for an inviscid, nonconducting gas. The only essential simplifications to this system of equations are a reduction in spatial dimensions from three to two, and use of small-disturbance approximations in the far field of the machine.

Stream Surface Equations

Consider a flow annulus as sketched in Fig. 1. The curvilinear distance along the intersection of the midline of the annulus with a meridional plane is termed the meridional distance m. The distance normal to the midline in a meridional plane is denoted by n, and the circumferential coordinate by θ. The thickness of the annulus b is assumed to be small compared to the radius r; hence the n component of the velocity vector and all variations in the n direction are neglected. Accordingly, the annulus is termed a stream surface. Transformation of the basic equations to the two-dimensional stream surface coordinate system is outlined in Ref. 3. In the analysis of the flow through a rotating blade row it is advantageous to express the governing equations in a relative coordinate system which rotates with the blades. Therefore, the following additional coordinate transformation is introduced:

$$x = m \tag{1}$$

$$y = r(\theta - \Omega t), \text{ at } x = \text{constant} \tag{2}$$

and the velocity components in the x,y,t system are correspondingly defined:

$$u = V_m \tag{3}$$

$$v = V_\theta - \Omega r \tag{4}$$

A relative total enthalpy§ and relative total energy are defined as:

$$H' = H - \Omega r V_\theta \tag{5}$$

$$E' = H' - p/\rho \tag{6}$$

The following system of equations is thereby obtained:

$$\frac{\partial \rho}{\partial t} + \frac{\partial \rho u}{\partial x} + \frac{\partial \rho v}{\partial y} = -\frac{\rho u}{rb}\frac{\mathrm{d}rb}{\mathrm{d}x} \tag{7}$$

§Sometimes referred to as "rothalpy" since it is *not* the total enthalpy which would be measured in the rotating frame of reference.

$$\frac{\partial \rho u}{\partial t}+\frac{\partial(\rho u^2+p)}{\partial x}+\frac{\partial \rho uv}{\partial y}=-\frac{\rho u^2}{rb}\frac{\mathrm{d}rb}{\mathrm{d}x}+\rho(v+\Omega r)^2\frac{1}{r}\frac{\mathrm{d}r}{\mathrm{d}x} \quad (8)$$

$$\frac{\partial \rho v}{\partial t}+\frac{\partial \rho uv}{\partial x}+\frac{\partial(\rho v^2+p)}{\partial y}=-\frac{\rho uv}{rb}\frac{\mathrm{d}rb}{\mathrm{d}x}-\rho u(v+2\Omega r)\frac{1}{r}\frac{\mathrm{d}r}{\mathrm{d}x} \quad (9)$$

and,

$$\frac{\partial \rho E'}{\partial t}+\frac{\partial \rho uH'}{\partial x}+\frac{\partial \rho vH'}{\partial y}=-\frac{\rho uH'}{rb}\frac{\mathrm{d}rb}{\mathrm{d}x} \quad (10a)$$

or,

$$\frac{\partial S}{\partial t}+u\frac{\partial S}{\partial x}+v\frac{\partial S}{\partial y}=0 \quad (10b)$$

$$p=\rho RT=(\gamma-1)\rho e=p_\infty(\rho/\rho_\infty)^\gamma\exp(\Delta S/C_v) \quad (11)$$

Note that the preceding system of equations can be applied in the relative (rotating) frame as stated, or in an absolute (stationary) frame by setting $\Omega=0$. In addition, the standard two-dimensional equations of motion are recovered when r and b are constants.

Description of the Computational Domain

As shown in Fig. 1, the region in which the computation is carried out consists of up to seven domains, which contain the two blade rows and segments of the stream surface extending upstream and downstream of the rows. (However, it is not necessary to include both blade rows or all seven domains in every case.) $N_2 \geq N_1$ is assumed, in conformity with standard compressor design procedure. The frame of reference of domains 1 through 4 is attached to the first blade row and that of domains 5 through 7 is attached to the second row. The solution in each domain is correspondingly carried out in a relative or absolute frame of reference. The lateral boundaries of domains 1 and 2 lie on straight-line projections of the mean camber line at the leading edge of the first blade row. The lateral boundaries of domains 3 and 5 are the blade surfaces, $y_u(m)$ and $y_\ell(m)$. The lateral boundaries of domains 4, 6, and 7 are the instantaneous locations of the blade slipstreams, $y_s(m,t)$.

Each domain is mapped from its shape in physical space into a unit square by defining stretched meridional and circumferential coordinates, σ and ν, given by

$$\sigma=\frac{x-x_i}{x_{i+1}-x_i} \quad \text{(in the } i\text{th domain)} \quad (12)$$

$$\nu=\frac{y-y_\ell}{y_u-y_\ell} \quad (13)$$

where x_i refers to the location of the upstream boundary of the ith domain.

Interior Point Solution Algorithm

Each of the seven computational domains is spanned by a rectangular grid network, having a mesh size of $\Delta\sigma$ by $\Delta\nu$:

$$\Delta\sigma=1/(JS-2) \quad (14)$$

$$\Delta\nu=1/(KS-4) \quad (15)$$

The grid ordering system is illustrated in Fig. 2. The grid rows $k=4$ and KS correspond to the circumferential boundaries of the blade-to-blade passage $y=y_\ell$ and y_u. The grid rows $K=1$, 2, and 3 and $K=KS+1$, $KS+2$, and $KS+3$ are exterior to the computational domain and are reserved for the solution in portions of the adjacent blade-to-blade passages. The rows $K=3$ and 4 occupy the same locations on the transformed boundary $\nu=0$. The rows $k=KS$ and $KS+1$ correspondingly occupy the same boundary $\nu=1$. On the slipstream these points also occupy the same physical locations. This convention was adopted in view of the anticipated discontinuities across the blade slipstreams.

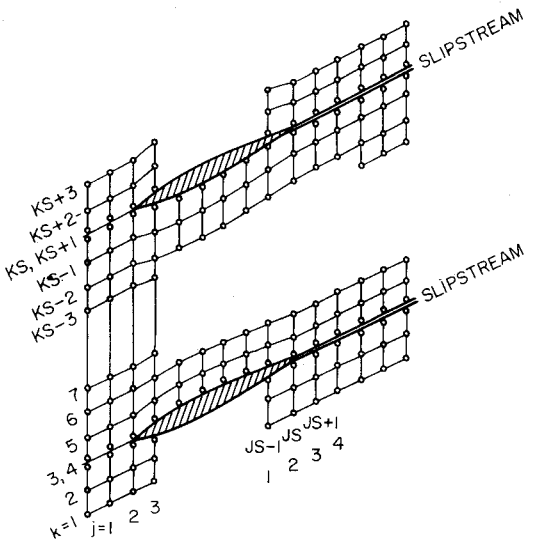

Fig. 2 Grid row ordering in vicinity of blades and slipstreams.

The finite-difference algorithm developed by MacCormack[4] is employed to carry out the solution at the interior grid points. The MacCormack algorithm achieves satisfactory stability without introduction of artificial damping terms or numerical filtering procedures.

Time is advanced in increments of Δt determined by a combination of stability and blade motion constraints. The well-known CFL criterion places an upper limit on the permissible time step. However, the application of boundary conditions in the case of unequal numbers of blades in the two blade rows is based on a phase lag in time (which will be discussed later). Implementation of the phase relations requires a constant value of Δt; therefore, an estimate of the maximum anticipated values of $u+a$ and $v+a$ must be made to determine the allowable step size Δt. In addition, the value must then be reduced such that the time for one blade of the second row to cross a single passage of the first row is an integer number of time steps.

Inlet and Discharge Boundary Conditions and Boundary Point Solution Algorithm

The present formulation assumes that the periodicity of the flowfield results entirely from the interaction of the rotor and stator blade rows. Accordingly, any nonuniformity, either spatial or timewise, of the properties of the flow crossing the inlet or discharge station attributable to inward traveling waves or inward convection must be ruled out. Identification of the flow properties which propagate by convection and by wave motion is facilitated by recasting the system of equations in characteristic form.

The characteristic surfaces formed by the present system of partial differential equations consists of a conoid with its base on the xy plane and within it a stream path which intersects the conoid at its vertex. A particularly useful approximation to the true characteristic form is obtained by stating the system of equations in a reference plane coordinate system which reduces the problem to a more tractable two-dimensional form.[5] If the reference plane is normal to both the xy plane ($t=$ constant) and the inlet station ($x=$ constant) and is allowed to translate the y direction at the same velocity as the circumferential component of gas velocity v, then (as will be shown) the system of characteristic lines illustrated in Fig. 3 is obtained. (Translation of the reference plane at the velocity v in effect transforms a rotating frame of reference back to an absolute frame. Thus, the inlet and discharge

station solutions are effectively carried out in an absolute frame regardless of the relative motion of the computational domains.)

The energy equation as given by Eq. (10b) is already in characteristic form; it can be integrated to yield

$$S=\text{constant, on}\frac{dx}{u}=\frac{dy}{v}=dt \tag{16}$$

which states the well-known fact that the entropy is convected on stream paths. Specifically, the entropy convects inward (assuming $u>0$) across the inlet station and outward across the discharge station. The condition $S=$ constant everywhere upstream of the inlet station forms the first boundary condition to be applied at the inlet. (It is assumed that any shock waves reaching the inlet station are sufficiently weak to be considered isentropic.)

If $\nabla S=0$, as at the inlet, then the curl of the momentum equation yields the vorticity transport equation. In terms of the presently considered two-dimensional system, the only nonzero component of vorticity is the radial component $\zeta=(\partial v/\partial x-\partial u/\partial y)$. The vorticity equation therefore yields

$$\frac{\zeta}{\rho}=\text{constant, on}\frac{dx}{u}=\frac{dy}{v}=dt \tag{17}$$

Thus, the ratio of vorticity to density also convects on stream paths. The condition $\zeta=0$ upstream of the inlet station is taken as the second boundary condition to be applied at the inlet station.

Equations (7, 8, 10b, and 11) can be combined to obtain

$$\frac{a}{\gamma p}\frac{dp}{dt}\pm\frac{du}{dt}=-a\left(\frac{\partial v}{\partial y}+\frac{u}{rb}\frac{drb}{dx}\right)$$

$$\pm(v+\Omega r)^2\frac{1}{r}\frac{dr}{dx},\ \text{on}\ \frac{dx}{u\pm a}=\frac{dy}{v}=dt \tag{18}$$

which provides a pair of compatibility relations which apply on the line AO and CO in Fig. 3.

Two limiting cases have been considered to be descriptive of the duct configuration at the inlet or discharge station. One case is an infinite duct, i.e., the inlet or discharge station is located in a region of constant cross-sectional area which extends "very far" outward from the inlet or discharge station. Consequently, all outward radiating waves should pass the inlet or discharge station without reflection in this case. Modeling of this condition will be discussed later. The second case represents the opposite limit in which all pressure waves are reflected at the inlet or discharge station; this case is termed an open-end duct, corresponding to the type of reflection associated with the open end of an organ pipe. The boundary condition, in this case, is that the pressure matches the plenum pressure outside the duct, namely,

$$p_{\text{inlet}}(y,t)=p_{-\infty} \tag{19}$$

$$p_{\text{discharge}}(y,t)=p_{\infty} \tag{20}$$

where the subscripts $\pm\infty$ denote $x>x_{\text{discharge}}$ and $x<x_{\text{inlet}}$, respectively.

Modeling of the nonreflective condition for an infinite duct is somewhat more complex, particularly in regard to the swirling waves produced by a rotor-stator interaction. A precise mathematical formulation of the flowfield solution upstream of the inlet station and downstream of the discharge station based on a small-perturbation analysis is described in Ref. 6 and provides an appropriate acoustic far-field model for an infinite duct. It accomplishes the desired objective of allowing an arbitrary transient signal to radiate outward without reflection and asymptotic attainment of a periodic solution with as many harmonic components as can be derived from the number of grid points spanning the considered boundaries.

An approximate model of the infinite duct condition has been developed which does not require use of acoustic far-field analysis. In the approximate model, the infinite duct conditions are derived from the wave-motion characteristics represented by Eq. (18). Consequently, the discrete acoustic modes are not explicitly identified in the approximate model, and their unimpeded transmission across the boundary cannot be guaranteed. In the approximate infinite duct model, Eq. (18) is integrated to yield

$$\frac{2a}{\gamma-1}\pm u=\int(-aQ_1\pm Q_2)\,dt+\text{constant},$$

$$\text{on}\ \frac{dx}{u\pm a}=\frac{dy}{v}=dt \tag{21}$$

Outside the computational domain $r=$ constant and $b=$ constant is assumed. The remaining term in the integrand of Eq. (21), namely $a\partial v/\partial y$, accounts for the two dimensionality of the actual wave surfaces, as compared to the one-dimensional (helical) surfaces which would result if the swirl component of velocity v were constant or only a function of x. If $\partial v/\partial y$ is neglected outside the computational domain, then the well-known Riemann invariants for the incoming waves are obtained from Eq. (21):

$$\left[\frac{2a(y,t)}{\gamma-1}+u(y,t)\right]_{\text{inlet}}=\frac{2a_{-\infty}}{\gamma-1}+u_{-\infty} \tag{22}$$

$$\left[\frac{2a(y,t)}{\gamma-1}-u(y,t)\right]_{\text{discharge}}=\frac{2a_{\infty}}{\gamma-1}-u_{\infty} \tag{23}$$

In this case the subscripts denote the specified values for $x\to\pm\infty$. The two dimensionality of the outward radiating waves at the inlet or discharge station is retained by evaluating the integrand of Eq. (21) numerically along the lines AO and CO in Fig. 3.

Determination of the swirl component of velocity at the boundary points at time $t+\Delta t$ can be accomplished by use of

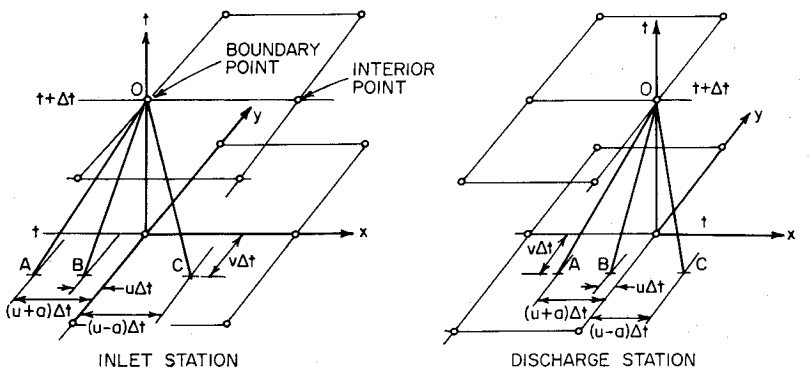

Fig. 3 Characteristic lines and grid points at inlet and discharge stations.

the circumferential momentum equation in the form

$$\frac{\partial v}{\partial t} = -\frac{\partial H'}{\partial y} + T\frac{\partial S}{\partial y} - u\zeta \tag{24}$$

Equation (24) does not involve any streamwise gradients (if ζ is known) and can, therefore, be evaluated along the inlet or discharge boundary by the same finite-difference algorithm employed at the interior points.

Summarizing, the inlet solution algorithm consists of the stated boundary conditions, namely: $S_{-\infty} = \text{constant}$, $\zeta_{-\infty} = 0$, and either $p_{-\infty} = \text{constant}$ (open duct) or $2a_{-\infty}/(\gamma-1) + u_{-\infty} = \text{constant}$ (infinite duct), together with the compatibility equation on the upstream wave, given by Eq. (21) with the minus sign, and the circumferential momentum equation, given by Eq. (24).

The considerations pertaining to formulation and statement of the discharge station boundary conditions and solution algorithm are similar to those outlined earlier. However, as indicated in Fig. 3, points A and B originate within the computational domain, and point C falls outside. Therefore, the compatibility relation pertaining to point C is replaced by a boundary condition given by either Eq. (20) or Eq. (23). Equation (16) is evaluated on the stream path B in this case, using linear interpolation. Solution of Eq. (24) is carried out using a first-order upstream difference to evaluate the σ derivatives necessary to compute ζ at the discharge boundary points.

Blade Surface and Slipstream Boundary Conditions and Solution Algorithm

The boundary condition at the blade surface is simply impermeability of the surface, which only requires that the component of velocity normal to the surface vanish. The blades are assumed to be thin and have sharp leading and trailing edges, as is typical of high-speed compressor and fan blades. Therefore, the Kutta condition, which requires the pressure to be continuous and finite at the trailing edge, is applicable. This also implies that the slipstream which emanates from the blade must originate at the trailing edge. Since the blade leading edge is sharp, and the incidence angles are not expected to be large, the streamline which wets the blade surface is assumed to intersect the leading edge. Accordingly, the leading-edge pressure is also required to be finite, but not continuous. Implementation of these conditions is described in Ref. 2.

It can be shown from application of the conservation form of the governing equations at an impermeable contact surface that the pressure must be continuous across the slipstream, and that the component of velocity normal to the slipstream surface must also be continuous and equal to the surface velocity. However, the tangential component of velocity may be discontinuous across the slipstream, as well as the density or other thermodynamic properties. These jumps (discontinuities) in flow properties result from unsteady variations in the work performed by the blades, or by differences in shock-produced losses on either side of the blade under steady conditions, for example. It is emphasized that the conservation form of the equations admit the existence of these jumps across a slipstream, but their magnitudes are not derivable from application of the conservation form of the governing equations to a surface of discontinuity. By contrast, the magnitude of the jumps across a shock wave result from solution of the Rankine-Hugoniot relations. Therefore, the slipstreams cannot be expected to evolve from a finite-difference solution of the governing equations in the same way that shock surfaces are "captured." Consequently, if the slipstream jumps and the corresponding slipstream motion are to be resolved accurately, the slipstreams must be explicitly recognized as surfaces of discontinuity, as they are in the present formulation.

The solution algorithms used at the blade surface and slipstream points are closely related and, therefore, will be derived for the more general case of the slipstream points. The result will then be specialized to the blade surface points.

A surface-oriented coordinate system $(\bar{x},\bar{y},t)$, as sketched in Fig. 4, is defined, with velocity components $(\bar{u},\bar{v})$. In this system, a pair of compatability relations analogous to those previously discussed in connection with the inlet and discharge boundaries can be obtained:

$$\frac{a}{\gamma p}\frac{dp}{dt} \pm \frac{d\bar{v}}{dt} = -a\left(\frac{\partial \bar{u}}{\partial \bar{x}} + \frac{\bar{v}}{R} + \frac{u}{rb}\frac{drb}{dx}\right)$$

$$\pm\left\{\frac{\bar{u}^2}{R} - \bar{u}\frac{\partial \phi}{\partial t} - \frac{1}{r}\frac{dr}{dx}[u(v+2\Omega r)\cos\phi + (v+\Omega r)^2\sin\phi]\right\},$$

$$\text{on } \frac{d\bar{x}}{u} = \frac{d\bar{y}}{\bar{v}\pm a} = dt \tag{25}$$

Implementation of the numerical solution of Eq. (25) is facilitated by introduction of an additional coordinate transformation from the curvilinear $(\bar{x},\bar{y})$ system to a series of local Cartesian systems (ξ,η) each of which is tangent to a grid point on the slipstream (or blade surface). The (ξ,η) system is shown schematically in Fig. 4. Note that in the (ξ,η) system $R^{-1} = \partial\phi/\partial t = 0$. The velocity components $(\bar{u},\bar{v})$ at the grid point at which the local (ξ,η) system is defined are unchanged by this transformation; however, their values at adjacent grid points must be evaluated with respect to the angle ϕ at the subject grid point. The overall effect of these transformations is to make evaluation of Eq. (25) closely approximate impingement of a one-dimensional acoustic wave on a surface which is moving at a velocity $\bar{v}$. Although

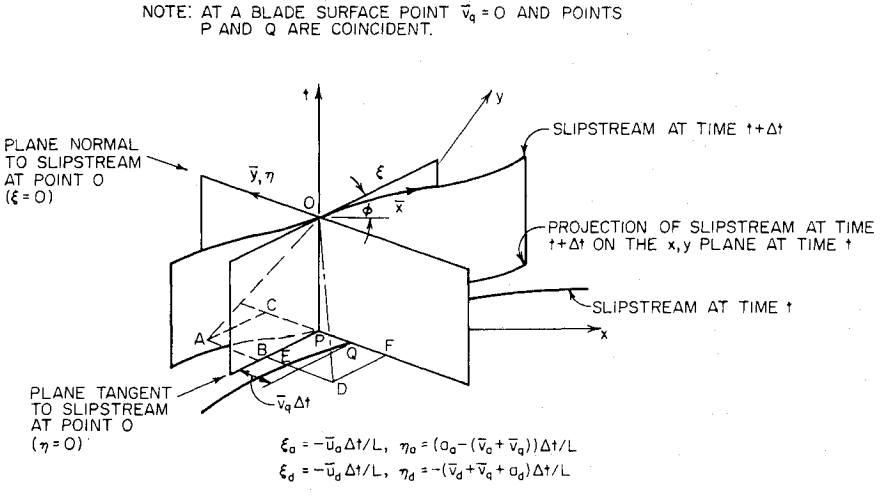

Fig. 4 Characteristic construction at a slipstream point.

all two-dimensional terms are in fact retained, they can be viewed as "corrections" to a more familiar one-dimensional solution.

The boundary point algorithm is completed by stating the streamwise momentum equation and the energy equation in the curvilinear $(\bar{x},\bar{y})$ system which follows a stream path along the moving surface:

$$\frac{DH'}{Dt} = \frac{1}{\rho}\frac{\partial p}{\partial t} \tag{26}$$

where

$$\frac{D}{Dt} = \frac{\partial}{\partial t} + \bar{u}\frac{\partial}{\partial \bar{x}} + \bar{v}\frac{\partial}{\partial \bar{y}} = \frac{\partial}{\partial t} + \bar{q}\frac{\partial}{\partial \bar{s}} \tag{27}$$

$$\bar{q} = (\bar{u}^2 + \bar{v}^2)^{1/2} \tag{28}$$

and

$$S = \text{constant on} \frac{d\bar{s}}{\bar{q}} = \frac{d\bar{x}}{\bar{u}} = \frac{d\bar{y}}{\bar{v}} = dt \tag{29}$$

Note that since Eq. (10b) has been used to represent conservation of energy, Eq. (10a) can be used to represent conservation of momentum in lieu of Eq. (8). Either form should be equivalent, but Eq. (10a) offers an advantageous form for numerical evaluation. In the present formulation, the pressure at time $t+\Delta t$ (point 0 in Fig. 4) is determined from the solution of Eq. (25), which is uncoupled from Eq. (26) and therefore can be evaluated first. Thus, the pressure derivative in Eq. (26) can be accurately approximated by

$$\frac{1}{\rho}\frac{\partial p}{\partial t} = \frac{2(p_0 - p_q)}{(\rho_0 + \rho_q)\Delta t} \tag{30}$$

Accordingly, Eq. (26) integrates to

$$H' = \text{constant} + \frac{2(p_0 - p_q)}{(\rho_0 + \rho_q)}, \text{ on } \frac{d\bar{s}}{\bar{q}} = \frac{d\bar{x}}{\bar{u}} = \frac{d\bar{y}}{\bar{v}} = dt \tag{31}$$

The constants indicated in Eqs. (29) and (31) are determined by evaluating S and H', respectively, at a distance $\Delta\bar{s} = \bar{q}\Delta t$ upstream of the point Q (in Fig. 4).

The values obtained for $\bar{v}$ on the slipstream are used to locate the new position of the slipstream for the next time step as follows:

$$x_n = x_0 - (\bar{v}\sin\phi)\Delta t \tag{32}$$

$$y_n = y_0 + (\bar{v}\cos\phi)\Delta t \tag{33}$$

where $[x_0, y_0(t)]$ are the coordinates of the slipstream point at which the just described solution is obtained, and (x_n, y_n) are its new coordinates. Linear interpolation is then used to find the new y coordinate, y_0 $(t+\Delta t)$ of the intersection of the slipstream and the grid column located at $x = x_0$, which are the coordinates of the slipstream grid point at the next time step.

The blade surface boundary condition is satisfied by setting $\bar{v} = 0$ at the blade surface grid points. In addition, at the trailing edge, the slipstream system is applicable subject to the constraint that $p_\ell = p_u$. This condition is satisfied by iterating the angle ϕ at the trailing edge, which, unlike ϕ at general blade surface and slipstream points, is not known a priori.

Special consideration must be given to the grid points at the intersections of the slipstreams and the discharge boundary, since these grid points lie on two boundaries of the computational domain. It should be emphasized in regard to these points that all the characteristic points (A, B, D, and E in Fig. 4) lie upstream of the subject point (assuming $\bar{u} > 0$). The numerical domain of dependence of a slipstream point, therefore, extends to the adjacent grid points only through the linear interpolations necessary to evaluate variables and derivatives at the characteristic points. This dependence represents the only mechanism by which those slipstream points which lie on the discharge boundary are affected by the discharge boundary conditions that are explicitly enforced at all other discharge boundary points.

Periodicity Condition

In the analysis of an isolated infinite cascade of blades in a uniform freestream, it is clear that the solution for the complete cascade will be steady (in the frame of reference of the blades) and have an angular period of $2\pi/N$. Enforcement of the periodicity condition is straightforward.

Numerical representation of the periodicity condition pertaining to conventional configurations, consisting of a pair of blade rows with the larger number of blades in the second row, has been accomplished by formulation of a cyclic procedure for equating the solution on the exterior grid rows identified earlier (i.e., $k = 1$, 2, 3 and $KS+1$, $KS+2$, $KS+3$) to that on corresponding interior rows (i.e., $k = KS-2$, $KS-1$, KS, and 4, 5, 6) at an earlier time through a set of appropriate phase relations. The same procedure is applied on the grid columns at the interface between domains 4 and 5.

An illustration of the nature of the cyclic procedure devised to enforce periodicity of the solution can be accomplished through use of the following simplified configurations.

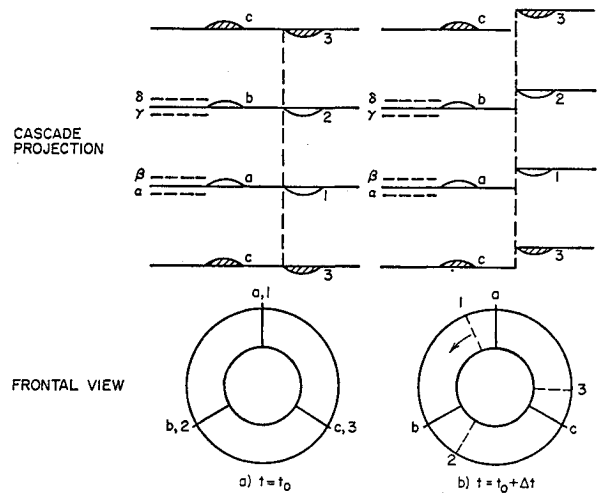

Fig. 5 Illustration of cyclic algorithm for stage with equal number of blades in stator and rotor ($N_1 = 3$, $N_2 = 3$).

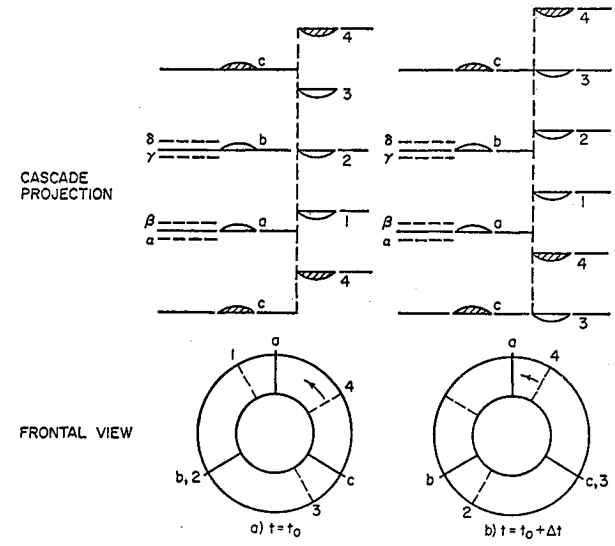

Fig. 6 Illustration of cyclic algorithm for stage with unequal number of blades in stator and rotor ($N_1 = 3$, $N_2 = 4$).

Consider first a stage having three rotor blades and three stator blades. For the present discussion, let the stator precede the rotor. This configuration is shown in Fig. 5, in both axial and cascade projections. At time t_0 all rotor and stator blades are aligned. It is clear in this case that the geometric boundary conditions (which determine the angular periodicity of the flow through the stage) are identical in each blade-to-blade passage at any time. Accordingly, the flowfield in each passage should be identical. In this case, the solution along an exterior grid row δ can be equated to that along the interior grid line β, and, similarly, that along the exterior line α can be equated to that along interior line γ, at any instant. Consider now the case with three blades in the stator and four blades in the rotor as shown in Fig. 6. At time t_0 rotor blade 2 is aligned with stator blade b, whereas at time $t_0+\Delta t$ rotor blade 3 is aligned with blade c. In this case, the instantaneous geometric conditions pertaining to the passage between blades a and b are obviously different from those for the passage between blades b and c. However, it may be noted that those pertaining to passage bc at $t_0+\Delta t$ are precisely the same as those which pertained to passage ab at the previous t_0. Therefore, the flow conditions along the exterior grid line δ at time $t_0+\Delta t$ can be equated to those along interior grid line β at the earlier time t_0. However, in this case those along the exterior grid line α at time $t_0+\Delta t$ cannot be equated to those occurring in passage ab at time t_0, but must be equated to those occurring along the line γ at an earlier time. Thus, a phase shift is introduced in application of the lateral boundary conditions. A detailed exposition of the cyclic procedure for application of the boundary conditions with appropriate phase shifts is contained in Ref. 2.

A similar procedure is used to define boundary values along the interface between domains 4 and 5. Sufficient data must be stored along this interface to provide information for a maximum period corresponding to the blade passing frequency of the first row (i.e., the row with the smaller number of blades). During this period the relative angular positions of the two domains will shift by $2\pi/N_1$. In addition, domain 4 will itself span an arc of $2\pi/N_1$; therefore, data covering a total arc of $2(2\pi/N_1)$ must be available. The boundary data are stored for one blade-to-blade passage on either side of the central passage which forms the computational domain, i.e., a total of three passages. Thus, for domain 5 the stored data span the arc $3(2\pi/N_2)$. An upper limit on the ratio of number of blades results, namely: $3/N_2 \geq 2/N_1$. The permissible number of blades in the second row is, therefore, bounded by

$$1 \leq \frac{N_2}{N_1} \leq \frac{3}{2} \tag{34}$$

The high-speed fan configurations considered to date[2] have stator to rotor ratios of the order of 1.05 and 1.12, which are within these limits.

Initial Conditions

In the present formulation, initial conditions can be specified in either of two ways. If no previous information is available the initial data for the entire computational domain are approximated from the inlet and discharge boundary conditions, (supplemented by $u_{-\infty}$ in the open-duct case) and an initial value of the swirl angle, $\tan^{-1} v/u$, at the inlet. If a previous solution, employing the same grid structure, is available it may be used as initial data, with either the same or revised boundary conditions.

It is also pointed out that the initial transient solution, which is physically irrelevant, can excite slipstream oscillations which are sufficiently violent to abort the computation. Therefore, provision has been included to utilize a "small-disturbance"-type slipstream approximation during the initial transient phase. In this case, the slipstream point algorithm is carried out in its entirety, but the resulting solution is applied on the original slipstream contour, which is held fixed. The computation of the slipstream motion is then restored after the initial transient phase of the interior solution has decayed.

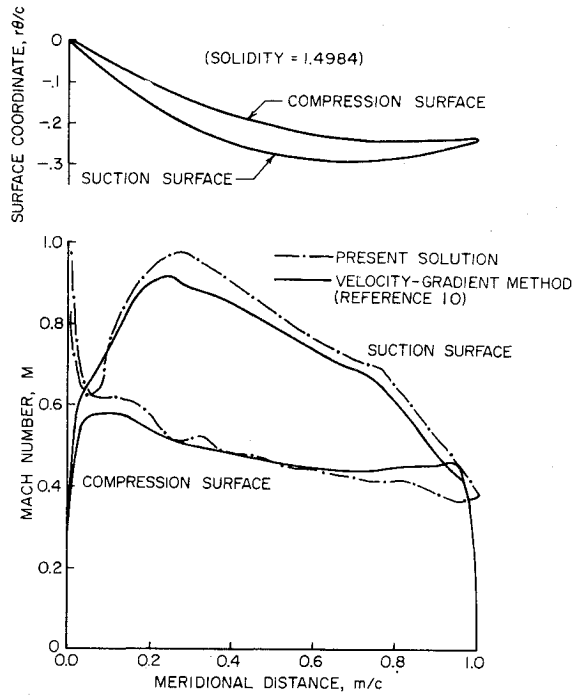

Fig. 7 Stator blade tip section geometry and comparison of surface Mach number distributions.

Results

The method of analysis just described has been implemented in a FORTRAN code[7] and tested with respect to a single-stage transonic fan for which experimental data are available.[8] A combination of design information and measured data for this fan has been used to define the initial and boundary conditions. The "infinite duct" inlet and discharge boundary conditions were used in the calculations reported here. The meridional plane analysis of Katsanis and McNally[9] was used to define the streamsheet thickness and radius by tracing a selected streamtube through the stage.

As a prelude to analysis of rotor-stator interactions, isolated rotor and isolated stator analyses were carried out. The stator analysis will be discussed first, since comparison of the present method and the finite-difference stream function method of Katsanis[10] is possible for this case, which offers a direct assessment of the program accuracy, independent of the viscous and three-dimensional effects present in the transonic rotor data. The experimental data[8] for the rotor will be used primarily to indicate the predictive capability of the present method with respect to the structure of passage shock systems.

The stator row has 46 blades and a hub-to-tip ratio of 0.6. The selected operating point corresponds to an open throttle, 100% speed condition (reading 137 of Ref. 8). The selected streamsheet follows the casing wall and has a thickness of ⅓ of 1% of the casing radius at the inlet station (one chord length upstream of the rotor). The inlet Mach number is 0.6 and the inlet flow angle is -30.7 deg. The stator is intended to produce a purely axial exit flow. The blade section at the casing is shown at the top of Fig. 7. A grid network consisting of 17 columns (axially) and 9 rows (circumferentially) in each of three domains (i.e., 459 points, excluding external grid points) was used for this case, as well as the isolated rotor case to be discussed next. The solutions converged within 10^3 time steps with this grid point density, and each required approximately 3-min execution time on a CDC 7600 computer.

An inlet Mach number of 0.65 and an inlet flow angle of −30.0 deg, with negligible circumferential variations, were obtained from the present stator solution. The outlet flow angle varied circumferentially from 6.6 to 7.0 deg. The relaxation solution was carried out for the same inlet Mach number of 0.65, but using the design inlet and exit flow angles of −30.7 deg and 0.0 deg, respectively. (Specification of the exit flow angle replaces the trailing-edge Kutta condition in the stream function method.[10]) Sixty-one grid columns and 20 grid rows were used in the stream function solution. The surface Mach number distributions are shown on the bottom of Fig. 7. It can be seen that the effect of nose bluntness (which is included in the stream function solution[10]) is essentially confined to the first 5-10% of the chord. The compression surface solutions are in quite good agreement up to the last 20% of chord, where the effect of the manner of enforcing the Kutta condition is evident. On the suction surface the present method results in a uniformly higher Mach number over almost all of the surface. In view of the doubled grid point density in the circumferential direction used in the stream function solution, it must be regarded as numerically more accurate.

The rotor for this stage has 44 blades and a hub-to-tip ratio of 0.5. The tip speed is 1500 fps, producing an inlet relative Mach number of 1.526 at the design point. The rotor has a shroud (vibration damper) located about 40% of span in from the tip. The stage also includes 24 variable camber inlet guide vanes, located slightly more than one rotor chord length upstream of the rotor. Under the presently considered conditions the guide vanes were set to zero camber, to produce a purely axial inlet flow to the rotor. The same open throttle, 100% speed operating point was selected, at which the stage total pressure ratio was 1.48 and inlet relative Mach number at the tip was 1.49. The streamsheet was again assumed to be a very narrow layer along casing wall (having a thickness of ⅓ of 1% of the radius).

An inlet Mach number of 1.47 was obtained in this case, and the rotor total pressure ratio varied (circumferentially) from 1.37 to 1.50, in good agreement with the design conditions. The rotor pressure contours obtained from the present solution compare favorably with those obtained[8] from arrays of fast-response pressure gages in the casing wall; a direct comparison is offered in Fig. 8. The differences near the leading edge are probably attributable to the effects of nose bluntness. The observed regions of compression-expansion preceding the passage shock ($z/c \simeq 0.7$ on the compression surface and $z/c \simeq 1.0$ on the suction surface) are indicative of local boundary-layer separation bubbles. The part-span shroud may also be generating a shock wave which interacts with blade shock system. In view of these factors, the general agreement between theory and experiment is regarded as quite satisfactory.

The rotor-stator interaction has also been examined at the open throttle, 100% speed operating point (reading 137 of Ref. 8). As pointed out, the stage has 44 rotor blades and 46 stator blades. Since the relative velocity leaving the rotor is supersonic ($M \simeq 1.1$), upstream propagation of disturbances from the stator should be cut off beyond the steady wave front intersecting the trailing edge of the lower rotor blade of the passage. If the flow were uniform in the passage, this wave front would intersect the upper rotor blade at about the 40% chord position; due to the nonuniformity of the flow it actually intersects the upper blade at between 60 and 80% of chord. The rotor flowfield upstream of this wave front converges rapidly to an essentially steady solution, whereas the stator is subjected to a sequence of perturbations which travel both upstream and downstream, and therefore converge to a periodic solution somewhat more slowly. The calculation was carried out for one complete revolution of the rotor, which required about 30 min of CDC 7600 computer time, using a grid network consisting of 12 grid columns and 9 grid rows in each of 5 domains. Approximately ¼ of a revolution (500 time steps) was required to achieve an asymptotic solution in the rotor passage, and about ½ revolution (1000 time steps) should have been sufficient to attain an asymptotic solution in the stator. Unfortunately, a minor coding error in the application of the phased boundary conditions was not discovered until ¾ of a revolution (1600 time steps) had been completed. Upon correction, a periodic

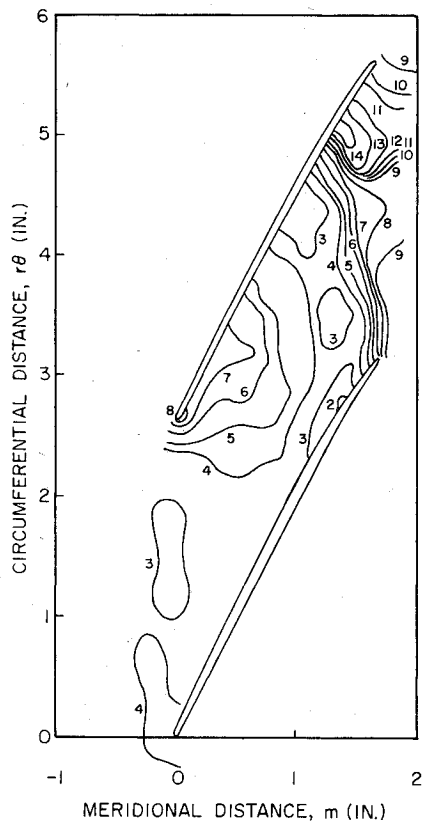

Fig. 8a Calculated static pressure contours at rotor tip.

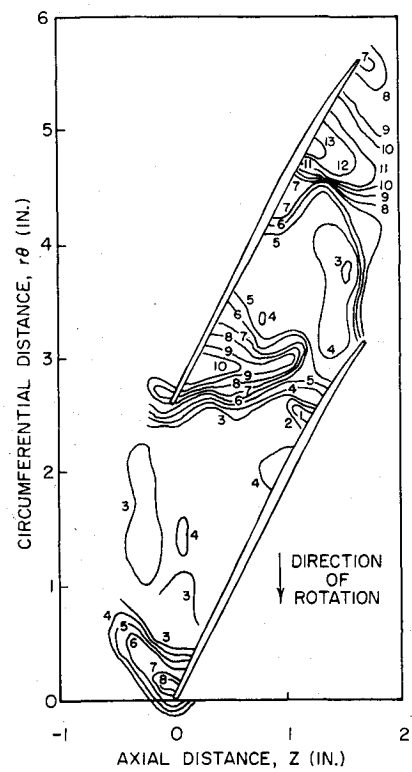

CONTOUR NUMBER	PRESSURE (PSIA)	(P/P_∞)
1	9	.7647
2	10	.8496
3	11	.9346
4	12	1.0195
5	13	1.1045
6	14	1.1895
7	15	1.2744
8	16	1.3594
9	17	1.4444
10	18	1.5293
11	19	1.6143
12	20	1.6992
13	21	1.7842

Fig. 8b Measured static pressure contours at rotor tip (reading 137 from Ref. 8).

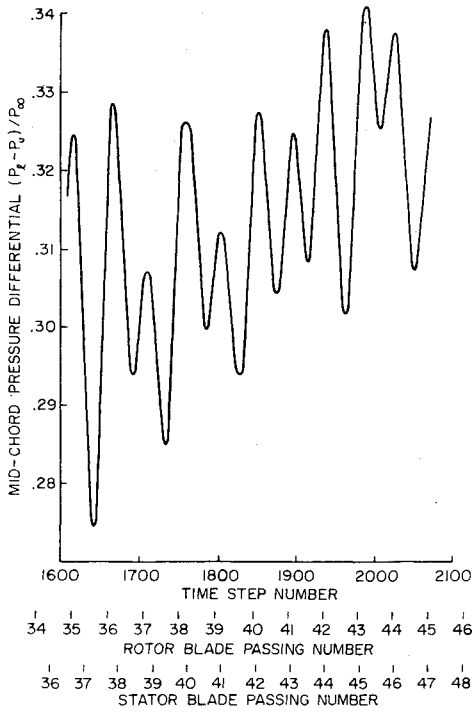

Fig. 9 Stator midchord pressure differential during quarter revolution of rotor.

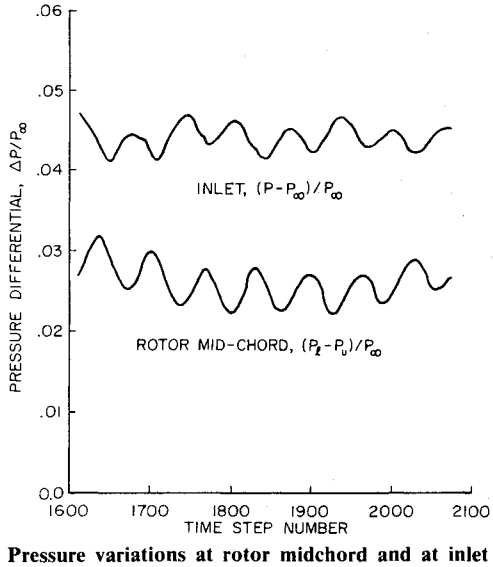

Fig. 10 Pressure variations at rotor midchord and at inlet during quarter revolution.

solution in the entire stage was achieved during the last ¼ of the revolution. The entire solution was not repeated due to the computing time requirement.

Provision to integrate the surface pressure distributions to obtain normal force and moment coefficients was not included in the code, making display of the periodic solution rather cumbersome. Therefore, the pressure difference across the blade at the midchord point has been selected to represent the blade force. The midchord pressure differential across the stator is shown in Fig. 9 for a period covering approximately the last ¼ of the rotor revolution. Presence of a periodic solution formed by superposition of two very distinct waves is apparent. One wave appears to have a peak-to-peak frequency twice the rotor passing frequency, and the other has a peak-to-peak frequency twice the stator passing frequency (relative to the rotor). Fourier analysis of the solution over the period of ½ a revolution would be required to quantify the spectral components of the blade row interaction field.

As indicated, the asymptotic flowfield upstream of about the midchord position of the rotor should be steady in the rotating frame of reference of the rotor. However, as can be seen in Fig. 10, a periodic pressure differential across the rotor midchord location is obtained, and in fact even the inlet pressure distribution exhibits periodicity in the rotating coordinate system. However, the amplitude of these oscillations is much smaller than those found in the stator. In view of the noted supersonic character of the relative flow through the rotor, these oscillations must be attributed to numerical propagation. Once the oscillations produced by the stator reach the leading edge of the rotor they are correctly able to propagate upstream, since the axial velocity component is subsonic. This spurious numerical propagation could be eliminated by observing the correct domain of dependence in formation of the difference operator, along the lines of the type-dependent difference operator used in the relaxation method developed by Murman and Cole[11] or Jameson.[12]

Summary and Recommendations

A numerical method of solution for inviscid, periodic, transonic flow through a set of interacting cascades has been developed. Particular attention has been devoted to the statement and method of implementation of boundary conditions. The solution algorithms employed at the interior and boundary points of the computational grid have been described in detail.

Several numerical examples have been carried out to demonstrate the capabilities and limitations of the method. The results presented herein describe a stream surface along the casing of a 1500-fps transonic fan stage[8] at an open throttle, 100% speed operating point. The rotor and stator have been considered individually and in combination. The stator solution compares well with the stream function solution of Katsanis and McNally,[9] except for the effects of the small, but finite, nose bluntness which influences the first 5 to 10% of the blade surface (about 20 nose radii). Nevertheless, the accuracy of the present solution over the major portion of the blade appears quite good. Only 9 grid rows were used from blade to blade, and further improvement could probably be achieved with a finer grid network. However, inclusion of nose bluntness in the present model is recommended to increase the accuracy and range of applicability of the method.

Examination of the transonic rotor solution indicates generally good agreement with the overall shock system structure; however, boundary-layer separation effects on the blade surface, evident in the data, produce local departures from the predicted shock structure. The leading-edge shock is somewhat stronger than predicted by the present method, again attributable to the neglect of nose bluntness.

A transonic rotor-stator interaction case was carried out for one full revolution of the rotor. The rotor solution became asymptotic within the first ¼ revolution, in accord with the rate of convergence of the isolated rotor cases. Unfortunately, conclusions regarding the rate of convergence to a periodic solution were compromised by the presence of a minor coding error which was not detected during the first ¾ of the rotor revolution. A periodic solution was obtained in the stator during the final ¼ revolution, upon correction of the error. Integration of the instantaneous surface pressure distributions to obtain normal force and moment coefficients would facilitate interpretation of the results, and is therefore recommended, as well as Fourier analysis of these coefficients to identify attainment of an asymptotic state and to characterize the spectral content of their temporal variation. Additionally, numerical propagation of periodic disturbances through a supersonic portion of the rotor passage, which on the basis of the mathematical zones of influence should have been inaccessible to upstream traveling waves, has been noted. Alteration of the finite-difference operators to

eliminate or at least minimize spurious upstream propagation through supersonic zones by correctly observing the mathematical domains of dependence of the grid points is also suggested.

Acknowledgment

This work was performed under the sponsorship of NASA Lewis Research Center through Contract NAS3-16807.

References

[1] Slutsky, S., "Discrete Noise Generation and Propagation by a Fan Engine," *Proceedings, AFOSR-UTIAS Symposium on Aerodynamic Noise*, University of Toronto Press, May 1968, pp. 20-21.

[2] Erdos, J. and Alzner, E., "Computation of Unsteady Transonic Flows Through Rotating and Stationary Cascades, Vol. 1—Method of Analysis," NASA CR 2900, 1977.

[3] Vavra, M. H., *Aerothermodynamics and Flow in Turbomachines*, Wiley, New York, 1960, Chap. 12 and Appendix A3.

[4] MacCormack, R. W., "The Effect of Viscosity on Hypervelocity Impact Cratering," AIAA Paper 69-534, 1969.

[5] Moretti, G. and Abbett, M., "A Time-Dependent Computational Method for Blunt Body Flows," *AIAA Journal*, Vol. 4, Dec. 1966, pp. 2136-2144.

[6] Slutsky, S., Fischer, D., and Erdos, J., "Computation of Unsteady Transonic Flows Through Rotating and Stationary Cascades, Vol. III—Acoustic Far-Field Analysis," NASA CR 2902, 1977.

[7] Alzner, E. and Kalben, P., "Computation of Unsteady Transonic Flows Through Rotating and Stationary Cascades, Vol. II—User's Guide to FORTRAN Program B2DATL," NASA CR 2901, 1977.

[8] Bilwakesh, K. R., Koch, C. C., and Prince, D. C., "Evaluation of Range and Distortion Tolerance for High Mach Number Transonic Fan Stages," NASA CR-72880, June 1972.

[9] Katsanis, T. and McNally, W. D., "Revised FORTRAN Program for Calculating Velocities and Streamlines on the Hub-Shroud Midchannel Stream Surface of an Axial-Radial-, or Mixed-Flow Turbomachine or Annular Duct," NASA TN D 8430, March 1977.

[10] Katsanis, T., "FORTRAN Program for Calculating Transonic Velocities on a Blade-To-Blade Stream Surface of a Turbomachine," NASA TN D 5427, 1969.

[11] Murman, E. M. and Cole, J. D., "Calculation of Plane Steady Transonic Flows," *AIAA Journal*, Vol. 9, Jan. 1971, pp. 114-121.

[12] Jameson, A., "Numerical Calculation of the Three-Dimensional Transonic Flow Over a Yawed Wing," *Proceedings of the AIAA Computational Fluid Dynamics Conference*, July 1973, Palm Springs, Calif., pp. 18-23.